Geophysical Research Letters®

Roughness of Ice Shelves Is Correlated With Basal Melt Rates

Ray H. Watkins[1] [ID]**, Jeremy N. Bassis[2]** [ID]**, and M. D. Thouless[1]**

[1]Department of Materials Science and Engineering, University of Michigan, Ann Arbor, MI, USA, [2]Department of Climate and Space Sciences and Engineering, University of Michigan, Ann Arbor, MI, USA

Abstract Ice shelf collapse could trigger widespread retreat of marine-based portions of the Antarctic ice sheet. However, little is known about the processes that control the stability of ice shelves. Recent observations have revealed that ice shelves have topographic features that span a spectrum of wavelengths, including basal channels and crevasses. Here we use ground-penetrating radar data to quantify patterns of roughness within and between ice shelves. We find that roughness follows a power law with the scaling exponent approximately constant between ice shelves. However, the level of roughness varies by nearly an order of magnitude between ice shelves. Critically, we find that roughness strongly correlates with basal melt, suggesting that increased melt not only leads to larger melt channels, but also to increased fracturing, rifting and decreased ice shelf stability. This hints that the mechanical stability of ice shelves may be more tightly controlled by ocean forcing than previously thought.

Plain Language Summary The future stability of the Antarctic ice sheet is linked to the stability of floating portions of the ice sheet called ice shelves. There has been recent speculation that the collapse of ice shelves could trigger an acceleration of the discharge of grounded ice, resulting in an accelerated sea level rise. Observations show that the topography of ice shelves is related to features, such as melt channels and crevasses, that are a direct result of melting and fracturing. Here we use ground-penetrating data collected from various airborne survey campaigns to calculate roughness of seven ice shelves across Antarctica. We find that roughness varies considerably between ice shelves and that increased roughness strongly correlates with increased basal melt. This connection hints at a complex interplay between increased melt rates and roughening of ice shelves, and suggests that basal melt may trigger widespread fracturing, influencing the mechanical stability of ice shelves.

1. Introduction

Ice shelves—slabs of floating ice fed by flow from the grounded ice upstream—play a critical role in limiting the discharge of grounded ice from the Antarctic ice sheet into the ocean (Dupont & Alley, 2005; Gudmundsson, 2013; Pritchard et al., 2012; Shepherd et al., 2018). Because ice shelves are in contact with both the ocean and atmosphere, they are sensitive to atmospheric and oceanic warming. For example, the explosive melt-water related disintegration of the Larsen A and B ice shelves in 1995 and 2002, provide vivid illustrations of the speed with which ice shelves can disintegrate (Rott et al., 1996; T. Scambos et al., 2003; Robel & Banwell, 2019). Both of these events increased the amount of ice discharge into the ocean (T. A. Scambos, 2004; Rignot, 2004; Rignot et al., 2019), linking the demise of ice shelves directly with increased mass flux, and increased rise in global sea levels.

Although rising atmospheric temperatures are responsible for the meltwater driven collapse of sections of the Larsen ice shelf, the temperatures in many other parts of Antarctica, like the Amundsen Sea Embayment, remain cold and there is little sustained surface melting (Dixon, 2007; Trusel et al., 2013; Werner et al., 2018). Instead, thinning, grounding-line retreat, and the instability of these glaciers is connected with basal melt associated with the intrusion of warm ocean waters (Jenkins et al., 2018; Nakayama et al., 2019). Recent observations and simulations show that, in addition to eroding contact with the margins and pinning points, basal melt can sculpt complex and heterogeneous basal channels (Drews, 2015; Dutrieux et al., 2013, 2014; Gourmelen et al., 2017; Stanton et al., 2013). Similarly, deep basal crevasses that eventually penetrate the entire ice thickness and become rifts have also been observed across many ice shelves (Jeong et al., 2016; McGrath et al., 2012).

Rifts, crevasses and melt channels contribute to the overall topography and roughness, defined here as topographic variations in the ice thickness varying from crevasses to large melt channels and rifts, of ice shelves. However,

Table 1
List of Data Products Used in This Study

Data Name	Data Source	Reference
MCoRDS L2 Ice Thickness	Operation IceBridge	(Paden et al., 2010)
Pine Island Ice Shelf 2011	Geophysics Data Portal	(Vaughan et al., 2012)
Total Ice Thickness	ROSSETTA-Ice	(Das et al., 2020)
Average Basal Melt	Multiple Sources	(Liu et al., 2015)

Note. Additional information is shown in Table S1 in Supporting Information S1.

the connection—if any—between the processes responsible for these features remains poorly understood. One possibility is that increased basal melt results in decreased ice thickness, reducing the restraining lateral shear stresses and, potentially, allowing the ice shelf to become un-moored from pinning points (Still et al., 2018). This reduction in restraining forces could thus result in increased fracturing, and decreased mechanical stability (Favier et al., 2016). Thus, one hypothesis is that increased ocean forcing results in thinning, reducing buttressing and increasing crevassing and rifting. Similarly, formation of melt channels can alter the stress distribution within the ice, promoting basal and surface fractures and/or excavating existing basal crevasses (Alley et al., 2016; Bassis & Ma, 2015; Vaughan et al., 2012). This suggests the complementary hypothesis that ocean forcing may also directly increase fracture and failure of ice shelves through the formation of melt channels and/or excavation of basal crevasses, which have advected and deformed for decades, centuries (or longer) and which potentially take on a wide variety of shapes and sizes. Here, we use existing ground-penetrating radar measurements to characterize roughness of ice shelves and the relationship between roughness and basal melt for a suite of Antarctic ice shelves.

2. Methods

2.1. Data and Study Regions

We used ground-penetrating radar data from a variety of sources (Table 1) to determine the thickness of ice shelves. Most available data that cover the Pine Island, Ross, Thwaites, Dotson, Getz, Larsen C, and Filchner ice shelves were used. These ice shelves were chosen because multiple tracks covered the region, and because these regions provide contrasting environmental and glaciological conditions. For instance, the Pine Island and Thwaites ice shelves are subject to significant basal melting (Dutrieux et al., 2014; Shean et al., 2019; Webber et al., 2017), whereas the Ross and Filchner ice shelves are subject to colder ocean conditions and much lower melt rates (Dixon, 2007; Liu et al., 2015).

We performed a more detailed study of Pine Island and Ross because of the abundant data coverage for these two ice shelves, and because of the contrasting climatological forcing. For instance, Pine Island is subject to large basal melt rates along the grounding line that can exceed hundreds of meters per year (Dutrieux et al., 2013; Shean et al., 2019), resulting in an elevated average basal melt across the entire ice shelf (Liu et al., 2015). The increased melt rate has triggered grounding line retreat (Favier et al., 2014) and, potentially, increased iceberg calving (Arndt et al., 2018; Joughin et al., 2021; Liu et al., 2015). By contrast, the Ross ice shelf experiences much lower basal melt rates (Das et al., 2020), with stable grounding line positions.

2.2. Quantifying Roughness

We followed (Whitehouse, 2004), and defined roughness (in meters) as the square root of the integral of the power spectral density ⏓⏓⏓ :

$$R = \sqrt{\int_{k_1}^{k_2} S(k)\,dk} \tag{1}$$

where (1/m) represents the wavenumber, and (1/m), (1/m) represent the range of integration in wavenumber space. The range is related to the resolution of the data and length of tracks analyzed.
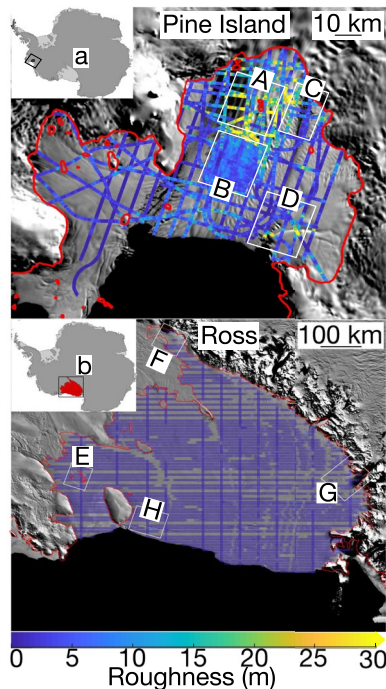
Figure 1. Spatial patterns of roughness for (a) the Pine Island ice shelf and (b) the Ross ice shelf. Roughness is color-coded and plotted over the MODIS Mosaic Image of Antarctica (Haran et al., 2014). Shown in red is the grounding line for each ice shelf obtained from NASA's MEaSUREs data-set (Rignot et al., 2013). Also boxes A-H are subsets of each ice shelf, which are shown in greater detail in Figure 2.

To calculate spatial variations in roughness across individual ice shelves, we first computed power spectra at windowed distances of size , set to 3000 m, and overlap percentage , set to ... . Roughness was then obtained through numerical integration of Equation 1 along each of the windows. Traditionally, the Fourier transform is used to estimate the power spectral density. However, we instead used a continuous wavelet transform, which produces improved along-track resolution by providing optimal basis functions that avoid spectral leakage when windowing the data (Sifuzzaman, 2009). This allowed us to resolve spatial variations in roughness at higher resolution.

We also computed the average roughness for each ice shelf by first computing the average power spectral density (obtained by averaging the spectra of all tracks), and then numerically integrating to find the average roughness. This approach has the advantage that it also provided an average spectrum for each ice shelf. We chose integration bounds between 0.0001 (1/m) for and 0.01111 (1/m) for k_2. This corresponds to looking at wavelengths between ~ 9 m and ~ 10 km, and was done so that we could consistently compare roughness between ice shelves of different dimensions. Our results are not sensitive to any windowing or scaling parameters when the parameters are varied over an order of magnitude. However, taking a track length much larger than 10 km, excluded a large number of tracks from the analysis. Moreover, we experimented with computing roughness and average roughness using a range of definitions, including just taking the mean of the windowed roughness measurements. Different definitions can influence the magnitude of roughness, but the trends and relative values are insensitive to any change in the definition of roughness used.

2.3. Spectral Characteristics of Roughness

If the power spectral density has peaks associated with features that have specific wavelengths, we can identify the dominant wavelength (or wavenumber) from the power spectra. Alternatively, the topography of many surfaces on Earth, Mars and Venus follow a power law over a range of wavelengths (Lovejoy, 1982; Mandelbrot & Wheeler, 1983). If the topography follows a power-law distribution, the power spectral density, takes the form:

$$PSD(k) = S(k) = Ck^{-\alpha}, \qquad (2)$$

where is a roughness scaling parameter, α is the power law (or fractal) exponent, and (1/m) is the wavenumber. The exponent α is commonly represented as the fractal dimension (Joe et al., 2017), with the relationship between α and expressed by $D = \frac{-\alpha + 8}{2}$.

We followed (Clauset et al., 2009) to estimate if the power spectral density could be described as a power law. If it could, we then estimated the scaling exponent α, including a minimum cutoff frequency into the fit of the exponent (Clauset et al., 2009) to account for limits in the resolution of our data. After estimating the exponent, we determined by preforming a least squares regression to the power law.

3. Results

3.1. Roughness of the Pine Island and Ross Ice Shelves

We first examined roughness of the Pine Island and Ross ice shelves. Roughness of Pine Island (Figure 1a) varies from close to ~ 0 m in the central portions and near the calving front to around ~ 60 m near the grounding line and pinning points. We see larger roughness in isolated regions of the ice shelf, corresponding to topographic features like pinning points (box A), melt channels (box B), crevasses in shear margins (box C), and rifts (box D). These structural features have all been previously documented in the ice shelf (Haran et al., 2014; Lhermitte et al., 2020; Vaughan et al., 2012), however it is also possible the rift in box D may have initiated in the shear margin before
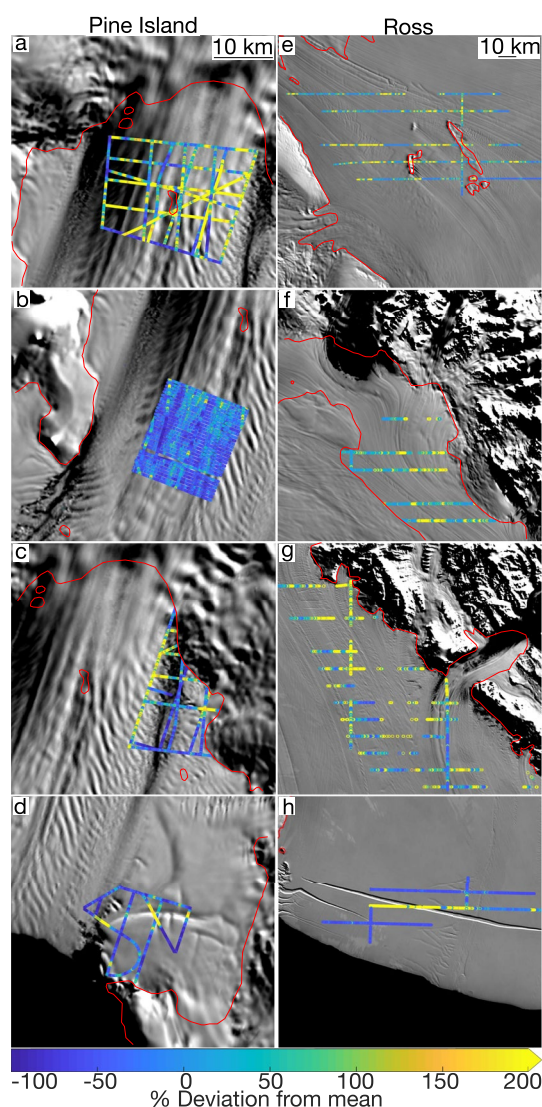
Figure 2. Percent deviation from the mean roughness for Pine Island (left) and Ross ice shelf (right). Panels a and e show pinning points. Panels b and f show melt channels. Panels c and g show shear margins. Panels d and h show rifts.

becoming a rift, indicating that classifying features is ambiguous. Similarly, the pinning point in box B may contain melt channels and crevasses Moreover, Pine Island may have retreated off the pinning point (box A) between 2009 and 2011 (Favier et al., 2014), and the elevated roughness may be a legacy of previous episodic grounding on and/or processes associated with un-mooring from the pinning point. (Note the pinning point we document is further upstream than the pinning point noted by (Jenkins et al., 2010)).

By contrast, roughness of the Ross ice shelf (Figure 1b) is much lower overall compared to Pine Island, with values rarely exceeding 10 m and it is less than 3 m on the majority of the ice shelf. Despite the smaller overall roughness of the Ross ice shelf, we still see elevated roughness relative to the mean for both ice shelves around pinning points, melt channels, shear margins and rifts (Figure 2). This is especially true for pinning points and shear margins (Figure S1 in Supporting Information S1). All of these structures create a topographic signature in roughness, but the magnitude varies substantially between ice shelves.

3.2. Average and Spectral Characteristics of Roughness

We see clear differences in the magnitude of roughness between the Pine Island and Ross ice shelves. Because pinning points, melt channels, crevasses, and rifts elevate roughness, we anticipated that the topography associated with these features would have characteristic spectral signatures. To investigate the spectral characteristics of roughness, we averaged the power spectral density for all the flight tracks over the Pine Island and Ross ice shelves (Figure 3). Contrary to our expectations, we do not see characteristic peaks in the power spectra corresponding to discrete wavelengths. Instead, the spectra for both Pine Island and Ross approximately followed power laws. Moreover, the power law exponent is statistically equivalent for both ice shelves, with the primary difference that the spectrum for Pine Island is shifted higher at *all* wavelengths compared to the Ross ice shelf.

We also characterized the average roughness for Pine Island and Ross by integrating over the average spectrum of each ice shelf between two wavenumber bounds (dashed lines in Figure 3). We found that the average roughness of Pine Island (55 m) was almost five times that of Ross (12 m). This result is consistent with our previous result in Figures 1 and 2, where we showed that roughness was consistently larger on Pine Island then the Ross ice shelf.

The power law behavior might be a consequence of the fact that tracks intersect with features at different angles, blurring out any characteristic peaks in the spectra. For Pine Island, where tracks are roughly oriented along-flow and transverse-to-flow, we also calculated the average transverse-to-flow roughness and the average longitudinal-to-flow roughness. The transverse-to-flow roughness was about twice as large as the longitudinal to flow roughness (66 vs. 30 m, Figure S2 in Supporting Information S1). In both cases however, the spectra of each approximately followed a power law with a statistically identical scaling exponent. This indicates that although Pine Island is experiencing increased basal and excavation of melt channels, which are seen mostly in the transverse to flow tracks, the increased roughness is not solely due to the increased prevalence of melt channels. Instead, transverse-to-flow features, like crevasses, are also introducing a larger component of roughness.

3.3. Roughness Is Highly Variable Between Ice Shelves, but the Power Law Exponent Is Constant

To determine if these results hold for a larger suite of ice shelves, we next extended our roughness analysis to five other Antarctic ice shelves: Thwaites, Dotson, Getz, Larsen C, and Filchner. Plots of the spectra and power law fits for the additional ice shelves can be found in Figure S3 in Supporting Information S1. We again
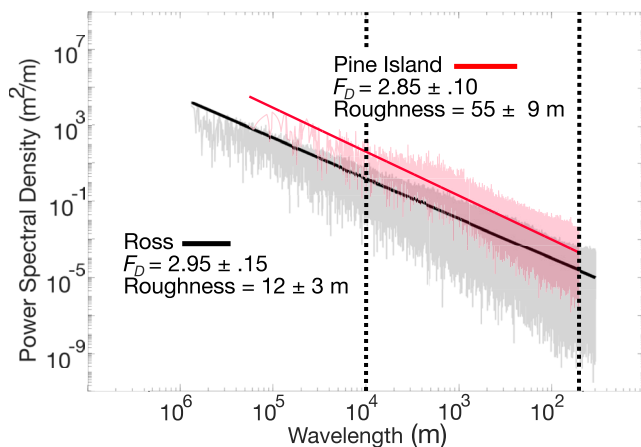
Figure 3. The power spectral density of all tracks going over the Pine Island and Ross ice shelves. Pine Island is plotted in light red and Ross is plotted in light gray. Also shown is a least squares fit of the power law equation to each spectrum. The solid red line represents the fit for Pine Island while the solid black line represents the fit for Ross. Integration bounds used for calculating the average roughness for each ice shelf are plotted by the black dotted lines.

found that the power law exponent was statistically identical for all of the ice shelves considered. However, the average roughness varied significantly (Figure 4). Measurements of the average roughness ranged over an order of magnitude, with a high of around 90 m for Thwaites and a low of around 12 m for Ross. However, we do see a pattern with larger roughness associated with ice shelves in the Amundsen Sea Embayment. We note that the Getz ice shelf may have slightly low roughness. However, given the small number of tracks, the low roughness of the Getz ice shelf is not statistically significant. Nonetheless, this low roughness may be due to its slow flow (Selley et al., 2021) and complex bathymetry constrained by multiple pinning points (Cochran et al., 2020).

3.4. The Average Roughness of Ice Shelves Is Correlated With Basal Melt Rates

Ice shelves in the Amundsen Sea Embayment have a larger roughness compared to other ice shelves (Figure 4). They also experience much larger basal melt rates due to the intrusion of warm water within the Amundsen Sea (Jenkins et al., 2018; Nakayama et al., 2019). To test for a connection with basal melt, we examined the relationship between the average basal melt rate, obtained from (Liu et al., 2015), and the average roughness of each ice shelf (Figure 5). We see a strong linear trend between increased basal melt and increased roughness. We also tested the effect of ice thickness on this trend and found that, even when the roughness is normalized with respect to the ice thickness, the strong linear trend remains. Crucially, this shows that basal melt correlates with—and perhaps triggers—increased roughness of the ice shelves. Intriguingly, based on its apparent power law nature, roughness also appears to increase across a broad spectrum of wavelengths, which may indicate a complex interplay between increased basal melt and ice dynamics.

4. Discussion

Our results show a clear relationship between pinning points and roughness (Figure 2 and Figure S1 in Supporting Information S1). Confining stresses associated with pinning points play a role nucleating crevasses and rifts and are involved in seeding the topographic expressions that eventually become rifts and melt channels (Still et al., 2018). Our results also show that roughness is increased relative to its *mean* over pinning points and other structural features, with very different roughness associated with these features between ice shelves (Figure 2 and Figure S1 in Supporting Information S1). This, combined with the correlation between roughness and basal melt, suggests basal melt might excavate localized topography, thereby enhancing roughness generated by pinning points and other features. Alternatively, refreezing in colder ocean environments, might fill topographic features,
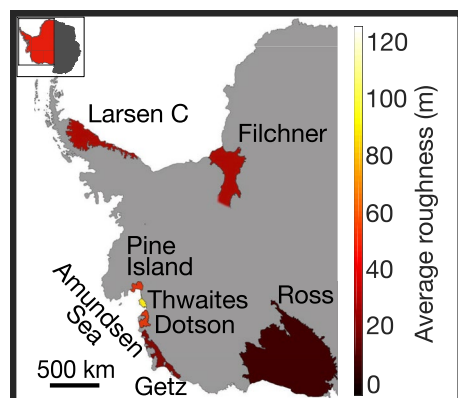

Figure 4. A mapping of roughness across several Antarctic ice shelves. Ice shelves are color coded to match up with the roughness axis.

smoothing out the surface. This is similar to the mechanism proposed by (Bassis & Ma, 2015) where increased ocean-forcing excavates crevasses resulting in deeper and wider features, which is the inverse of processes on ice shelves over colder water where observations show marine ice filling suture zones between ice streams (Holland et al., 2009; Luckman et al., 2012). This hypothesis, however, contrasts with high-resolution, two-dimensional models of ice-ocean interaction within crevasses (Jordan et al., 2014). These models show that the pressure-dependence of the basal melt rate results in lower melt rates or refreezing within crevasses, implying that the ocean will smooth out features. More work is needed to disentangle the mechanisms responsible for the amplification of topography on the 1–100 m scale, including (numerically expensive) three-dimensional models of circulation capable of resolving meter scale features.

Our results also indicate that roughness is strongly correlated with average basal melt rates beneath ice shelves. It is possible that the larger basal melt rates we observe are a direct consequence of the larger roughness. For example,
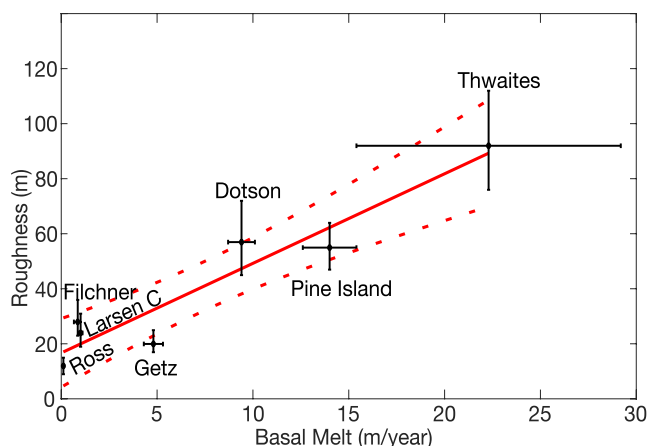
Figure 5. Least squares regression of basal melt and the average roughness of seven Antarctic ice shelves. Plotted in red is the best fit line with 2-σ confidence bounds.

the amount of energy transferred to the ice-ocean interface is often assumed to depend on roughness, albeit on millimeter-to-centimeter scales (Jenkins et al., 2010). Although the roughness-scale in turbulent energy transfer is much smaller than the scales we consider (and resolve), we also compared point estimates of roughness to basal melt rates (Adusumilli et al., 2020) for Pine Island, and found little correlation between basal melt rates across individual ice shelves and regions where the roughness across individual ice shelves is large (Figure S4 in Supporting Information S1). This implies that that the interplay between basal melt and roughness is the result of feedbacks that span large sections of ice shelves, rather than a purely localized response to increased basal melt. This hints that the increased roughness is at least partly caused by a change in the stress regime associated with increased basal. For example, increased basal melt may reduce contact with pinning points and lateral margins, resulting in decreased buttressing that promotes crevassing. At the same time, basal melt channels seed crevasses (Favier et al., 2014; Vaughan et al., 2012) and crevasses may become excavated over time to become larger features such as melt channels.

Although we are unable to resolve anisotropy or directionality of roughness, increased basal melt appears to be associated with increased roughness across all scales. Instead of finding a strong spectral signature associated with different features, rough ice shelves are rough across a large range of wavelengths. This is broadly consistent with our hypothesis that increased basal melt alters the stress regime of the shelf, but does challenge our classification of features into ''basal melt channels'' and "crevasses".

Our observations hint at complex interactions between the ice and ocean over a significant range of scales and features. Critically, however, roughness in ice shelves appears to be not only diagnostic of large basal melt rates, but correlates with ice shelves that are experiencing significant changes, including unpinning and grounding line migration (Favier et al., 2014; Milillo et al., 2019). This suggests that increased roughness may be an easily measurable proxy for ice shelf stability. Moreover, increasing roughness associated with fracture and failure of ice might point toward future vulnerabilities to ice shelves to collapse through increased fracture and failure. Given that current ice shelf models predict much smoother topography than our observations indicate, we need to better understand the source and evolution of the topographic signature of roughness to better understand these links.

5. Conclusions

We find that roughness varies significantly within and between ice shelves. Pinning points, crevasses, melt channels, and rifts all increase roughness of ice shelves. Additionally, we find that the average roughness of ice shelves has a strong correlation with basal melt, with Amundsen Sea ice shelves that have experienced stark increases in ocean forcing, exhibiting the highest roughness. Moreover, we also find that the average roughness spectra of ice shelves approximately follow a power law distribution with larger wavelength features having higher magnitude roughness, and smaller wavelength features having lower magnitude roughness. These results suggests that ocean-forcing is playing a dominant role in the evolution of roughness within and between ice shelves. The reason for this strong connection is less clear, but it hints that we will see continued transitions to rougher ice shelves as more ice shelves are subjected to increased basal melt rates. Crucially, the roughest ice shelves in our study have all experienced grounding line retreat and decreased buttressing, hinting at a direct connection between ocean forcing and the mechanical stability of ice shelves.

Data Availability Statement

Operation Ice-Bridge data sets used in this publication can be found at (https://nsidc.org/icebridge/portal/map). BAS data used for Pine Island is found at (https://secure.antarctica.ac.uk/data/aerogeo/index.php). ROSSETTA data used for the Ross ice shelf is found at (https://pgg.ldeo.columbia.edu/data/rosetta-ice). Mapping was done with the help of the Antarctic Mapping Toolbox in MATLAB (Greene et al., 2017).

References

Adusumilli, S., Fricker, H. A., Medley, B., Padman, L., & Siegfried, M. R. (2020). Interannual variations in meltwater input to the southern ocean from Antarctic ice shelves. *Nature Geoscience*, *13*(9), 616–620. https://doi.org/10.1038/s41561-020-0616-z

Alley, K. E., Scambos, T. A., Siegfried, M. R., & Fricker, H. A. (2016). Impacts of warm water on Antarctic ice shelf stability through basal channel formation. *Nature Geoscience*, *9*(4), 290–293. https://doi.org/10.1038/ngeo2675

Arndt, J. E., Larter, R. D., Friedl, P., Gohl, K., & Höppner., K. (2018). Bathymetric controls on calving processes at pine island glacier. *The Cryosphere*, *12*(6), 2039–2050. https://doi.org/10.5194/tc-12-2039-2018

Bassis, J., & Ma, Y. (2015). Evolution of basal crevasses links ice shelf stability to ocean forcing. *Earth and Planetary Science Letters*, *409*, 203–211. https://doi.org/10.1016/j.epsl.2014.11.003

Clauset, A., Shalizi, C. R., & Newman, M. E. J. (2009). Power-law distributions in empirical data. *SIAM Review*, *51*(4), 661–703. https://doi.org/10.1137/070710111

Cochran, J. R., Tinto, K. J., & Bell, R. E. (2020). Detailed bathymetry of the continental shelf beneath the getz ice shelf, west antarctica. *Journal of Geophysical Research: Earth Surface*, *125*(10). https://doi.org/10.1029/2019jf005493

Das, I., Padman, L., Bell, R. E., Fricker, H. A., Tinto, K. J., Hulbe, C. L., et al. (2020). Multi-decadal basal melt rates and structure of the Ross Ice Shelf, Antarctica using airborne ice penetrating radar. *Journal of Geophysical Research: Earth Surface*, *125*. https://doi.org/10.1029/2019JF005241

Dixon, D. (2007). (USAP-DC), via National Snow and Ice Data Center (NSIDC). *Antarctic mean annual temperature map*. U.S. Antarctic Program Data Center. Retrieved from http://www.usap-dc.org/view/dataset/609318

Drews, R. (2015). Evolution of ice-shelf channels in Antarctic ice shelves. *The Cryosphere*, *9*(3), 1169–1181. https://doi.org/10.5194/tc-9-1169-2015

Dupont, T. K., & Alley, R. B. (2005). Assessment of the importance of ice-shelf buttressing to ice-sheet flow. *Geophysical Research Letters*, *32*(4). https://doi.org/10.1029/2004gl022024

Dutrieux, P., Stewart, C., Jenkins, A., Nicholls, K. W., Corr, H. F. J., Rignot, E., & Steffen, K. (2014). Basal terraces on melting ice shelves. *Geophysical Research Letters*, *41*(15), 5506–5513. https://doi.org/10.1002/2014gl060618

Dutrieux, P., Vaughan, D. G., Corr, H. F. J., Jenkins, A., Holland, P. R., Joughin, I., & Fleming, A. H. (2013). Pine island glacier ice shelf melt distributed at kilometre scales. *The Cryosphere*, *7*(5), 1543–1555. https://doi.org/10.5194/tc-7-1543-2013

Favier, L., Durand, G., Cornford, S. L., Gudmundsson, G. H., Gagliardini, O., Gillet-Chaulet, F., & Brocq, A. M. L. (2014). Retreat of pine island glacier controlled by marine ice-sheet instability. *Nature Climate Change*, *4*(2), 117–121. https://doi.org/10.1038/nclimate2094

Favier, L., Pattyn, F., Berger, S., & Drews, R. (2016). Dynamic influence of pinning points on marine ice-sheet stability: A numerical study in dronning maud land, east Antarctica. *The Cryosphere*, *10*(6), 2623–2635. https://doi.org/10.5194/tc-10-2623-2016

Gourmelen, N., Goldberg, D. N., Snow, K., Henley, S. F., Bingham, R. G., Kimura, S., & Berg, W. J. (2017). Channelized melting drives thinning under a rapidly melting antarctic ice shelf. *Geophysical Research Letters*, *44*(19), 9796–9804. https://doi.org/10.1002/2017gl074929

Greene, C. A., Gwyther, D. E., & Blankenship, D. D. (2017). Antarctic mapping tools for matlab. *Computers & Geosciences*, *104*, 151–157. https://doi.org/10.1016/j.cageo.2016.08.003

Gudmundsson, G. H. (2013). Ice-shelf buttressing and the stability of marine ice sheets. *The Cryosphere*, *7*(2), 647–655. https://doi.org/10.5194/tc-7-647-2013

Haran, T., Bohlander, J., Scambos, T., Painter, T., & Fahnestock, M. (2014). *Modis mosaic of Antarctica 2008-2009 (moa2009) image map*. Digital media.

Holland, P. R., Corr, H. F. J., Vaughan, D. G., Jenkins, A., & Skvarca, P. (2009). June)Marine ice in larsen ice shelf. *Geophysical Research Letters*, *36*(11). https://doi.org/10.1029/2009gl038162

Jenkins, A., Nicholls, K. W., & Corr, H. F. J. (2010). Observation and parameterization of ablation at the base of ronne ice shelf, Antarctica. *Journal of Physical Oceanography*, *40*(10), 2298–2312. https://doi.org/10.1175/2010jpo4317.1

Jenkins, A., Shoosmith, D., Dutrieux, P., Jacobs, S., Kim, T. W., Lee, S. H., & Stammerjohn, S. (2018). West Antarctic ice sheet retreat in the Amundsen sea driven by decadal oceanic variability. *Nature Geoscience*, *11*(10), 733–738. https://doi.org/10.1038/s41561-018-0207-4

Jeong, S., Howat, I. M., & Bassis, J. N. (2016). Accelerated ice shelf rifting and retreat at pine island glacier, west Antarctica. *Geophysical Research Letters*, *43*(22). https://doi.org/10.1002/2016gl071360

Joe, J., Scaraggi, M., & Barber, J. (2017). Effect of fine-scale roughness on the tractions between contacting bodies. *Tribology International*, *111*, 52–56. https://doi.org/10.1016/j.triboint.2017.03.001

Jordan, J. R., Holland, P. R., Jenkins, A., Piggott, M. D., & Kimura, S. (2014). Modeling ice-ocean interaction in ice-shelf crevasses. *Journal of Geophysical Research: Oceans*, *119*(2), 995–1008. https://doi.org/10.1002/2013jc009208

Joughin, I., Shapero, D., Smith, B., Dutrieux, P., & Barham, M. (2021). Ice-shelf retreat drives recent pine island glacier speedup. *Science Advances*, *7*(24), eabg3080. https://doi.org/10.1126/sciadv.abg3080

Lhermitte, S., Sun, S., Shuman, C., Wouters, B., Pattyn, F., Wuite, J., & Nagler, T. (2020). Damage accelerates ice shelf instability and mass loss in Amundsen sea embayment. *Proceedings of the National Academy of Sciences*, *117*(40), 24735–24741. https://doi.org/10.1073/pnas.1912890117

Liu, Y., Moore, J. C., Cheng, X., Gladstone, R. M., Bassis, J. N., Liu, H., & Hui, F. (2015). Ocean-driven thinning enhances iceberg calving and retreat of Antarctic ice shelves. *Proceedings of the National Academy of Sciences*, *112*(11), 3263–3268. https://doi.org/10.1073/pnas.1415137112

Lovejoy, S. (1982). Area-perimeter relation for rain and cloud areas. *Science*, *216*(4542), 185–187. https://doi.org/10.1126/science.216.4542.185

Luckman, A., Jansen, D., Kulessa, B., King, E. C., Sammonds, P., & Benn, D. I. (2012). Basal crevasses in larsen c ice shelf and implications for their global abundance. *The Cryosphere*, *6*(1), 113–123. https://doi.org/10.5194/tc-6-113-2012

Mandelbrot, B. B., & Wheeler, J. A. (1983). The fractal geometry of nature. *American Journal of Physics*, *51*(3), 286–287. https://doi.org/10.1119/1.13295

McGrath, D., Steffen, K., Scambos, T., Rajaram, H., Casassa, G., & Lagos, J. L. R. (2012). Basal crevasses and associated surface crevassing on the larsen c ice shelf, Antarctica, and their role in ice-shelf instability. *Annals of Glaciology*, *53*(60), 10–18. https://doi.org/10.3189/2012aog60a005

Milillo, P., Rignot, E., Rizzoli, P., Scheuchl, B., Mouginot, J., Bueso-Bello, J., & Prats-Iraola, P. (2019). Heterogeneous retreat and ice melt of thwaites glacier, west antarctica. *Science Advances*, *5*(1), eaau3433. https://doi.org/10.1126/sciadv.aau3433

Nakayama, Y., Manucharyan, G., Zhang, H., Dutrieux, P., Torres, H. S., Klein, P., & Menemenlis, D. (2019). Pathways of ocean heat towards Pine Island and thwaites grounding lines. *Scientific Reports*, *9*(1). https://doi.org/10.1038/s41598-019-53190-6

Paden, J., Li, J., Leuschen, C., Rodriguez-Morales, F., & Hale, R. (2010). Icebridge mcords l2 ice thickness, version 1. *NASA National Snow and ice Data Center Distributed Active Archive Center*. https://doi.org/10.5067/gdq0cucvte2q

Pritchard, H. D., Ligtenberg, S. R. M., Fricker, H. A., Vaughan, D. G., van den Broeke, M. R., & Padman, L. (2012). Antarctic ice-sheet loss driven by basal melting of ice shelves. *Nature*, *484*(7395), 502–505. https://doi.org/10.1038/nature10968

Rignot, E. (2004). Accelerated ice discharge from the Antarctic peninsula following the collapse of larsen b ice shelf. *Geophysical Research Letters*, *31*(18). https://doi.org/10.1029/2004gl020697

Rignot, E., Jacobs, S., Mouginot, J., & Scheuchl, B. (2013). Ice-shelf melting around Antarctica. *Science*, *341*(6143), 266–270. https://doi.org/10.1126/science.1235798

Rignot, E., Mouginot, J., Scheuchl, B., van den Broeke, M., van Wessem, M. J., & Morlighem, M. (2019). Four decades of Antarctic ice sheet mass balance from 1979–2017. *Proceedings of the National Academy of Sciences*, *116*(4), 1095–1103. https://doi.org/10.1073/2Fpnas.1812883116

Robel, A. A., & Banwell, A. F. (2019). A speed limit on ice shelf collapse through hydrofracture. *Geophysical Research Letters*, *46*(21), 12092–12100. https://doi.org/10.1029/2019gl084397

Rott, H., Skvarca, P., & Nagler, T. (1996). Rapid collapse of northern Larsen ice shelf, Antarctica. *Science*, *271*(5250), 788–792. https://doi.org/10.1126/science.271.5250.788

Scambos, T., Hulbe, C., & Fahnestock, M. (2003). Climate-induced ice shelf disintegration in the Antarctic peninsula. In *Antarctic peninsula climate variability: Historical and paleoenvironmental perspectives* (pp. 79–92). American Geophysical Union. https://doi.org/10.1029/ar079p0079

Scambos, T. A. (2004). Glacier acceleration and thinning after ice shelf collapse in the larsen b embayment, Antarctica. *Geophysical Research Letters*, *31*(18). https://doi.org/10.1029/2004gl020670

Selley, H. L., Hogg, A. E., Cornford, S., Dutrieux, P., Shepherd, A., Wuite, J., & Kim, T.-W. (2021). Widespread increase in dynamic imbalance in the getz region of antarctica from 1994 to 2018. *Nature Communications*, *12*(1). https://doi.org/10.1038/s41467-021-21321-1

Shean, D. E., Joughin, I. R., Dutrieux, P., Smith, B. E., & Berthier, E. (2019). October). Ice shelf basal melt rates from a high-resolution digital elevation model (DEM) record for pine island glacier, Antarctica. *The Cryosphere*, *13*(10), 2633–2656. https://doi.org/10.5194/tc-13-2633-2019

Shepherd, A., Fricker, H. A., & Farrell, S. L. (2018). Trends and connections across the Antarctic cryosphere. *Nature*, *558*(7709), 223–232. https://doi.org/10.1038/s41586-018-0171-6

Sifuzzaman, M. (2009). *Application of wavelet transform and its advantages compared to fourier transform*.

Stanton, T. P., Shaw, W. J., Truffer, M., Corr, H. F. J., Peters, L. E., Riverman, K. L., & Anandakrishnan, S. (2013). Channelized ice melting in the ocean boundary layer beneath pine island glacier, Antarctica. *Science*, *341*(6151), 1236–1239. https://doi.org/10.1126/science.1239373

Still, H., Campbell, A., & Hulbe, C. (2018). Mechanical analysis of pinning points in the ross ice shelf, Antarctica. *Annals of Glaciology*, *60*(78), 32–41. https://doi.org/10.1017/aog.2018.31

Trusel, L. D., Frey, K. E., Das, S. B., Munneke, P. K., & van den Broeke, M. R. (2013). Satellite-based estimates of Antarctic surface meltwater fluxes. *Geophysical Research Letters*, *40*(23), 6148–6153. https://doi.org/10.1002/2013gl058138

Vaughan, D. G., Corr, H. F. J., Bindschadler, R. A., Dutrieux, P., Gudmundsson, G. H., Jenkins, A., & Wingham, D. J. (2012). Subglacial melt channels and fracture in the floating part of pine island glacier, Antarctica. *Journal of Geophysical Research: Earth Surface*, *117*(F3). https://doi.org/10.1029/2012jf002360

Webber, B. G. M., Heywood, K. J., Stevens, D. P., Dutrieux, P., Abrahamsen, E. P., Jenkins, A., & Kim, T. W. (2017). Mechanisms driving variability in the ocean forcing of pine island glacier. *Nature Communications*, *8*(1). https://doi.org/10.1038/ncomms14507

Werner, M., Jouzel, J., Masson-Delmotte, V., & Lohmann, G. (2018). Reconciling glacial antarctic water stable isotopes with ice sheet topography and the isotopic paleothermometer. *Nature Communications*, *9*(1). https://doi.org/10.1038/s41467-018-05430-y

Whitehouse, D. J. (2004). *Surfaces and their measurement*. Kogan Page Science.